Mechanisms for Power Deposition in Ar/SiH_4 Capacitively Coupled RF Discharges

MARK J. KUSHNER, MEMBER, IEEE

Abstract—In low-pressure capacitively coupled parallel-plate radio-frequency (RF) discharges, such as those used in plasma processing of semiconductor materials, power deposition and the rate of electron-impact excitation collisions depend upon time during the RF cycle and position in the discharge. Power is coupled into the discharge in at least two ways: by way of a high-energy "e-beam" component of the electron distribution resulting from electrons falling through or being accelerated by the oscillating sheaths, and by "joule heating" in the body of plasma. This paper will discuss the method of power deposition by electrons and the spatial dependence of electron-impact excitation rates in low-pressure capacitively coupled RF discharges with results from a Monte Carlo plasma simulation code. Mixtures of argon and silane will be examined as typical examples of discharges used for the plasma deposition of amorphous silicon.

I. Introduction

LOW-PRESSURE (<0.2 torr) parallel-plate capacitively coupled radio-frequency (RF) discharges are now commonly used for the plasma processing of semiconductor materials. Plasma etching [1] and plasma-enhanced chemical vapor deposition [2] (PECVD) are processes in which an RF discharge is used to provide the activation energy for chemical reactions in the gas phase. The products of the gas-phase reactions (heavy particle collisions and electron-impact excitation) are then transported to the semiconductor surface where they are adsorbed or otherwise react. The manner and location in which power is deposited in the discharge determines the rate of generation and type of radicals produced in the plasma and therefore determines the character of the etch or deposition. To optimize either process, the mechanisms for, and spatial dependence of, power deposition must be understood. This paper will address the issue of power deposition by electrons in capacitively coupled RF discharges in the parallel-plate geometry. We will examine the manner in which power is deposited in an RF plasma sustained in a gas mixture of Ar/SiH_4, typical of those used for the PECVD of amorphous silicon [2]. We will also discuss the spatial dependence of excitation rates within the discharge and relate them to the method of power deposition.

When an RF potential is applied to a capacitively coupled discharge, a large fraction of the voltage can appear across the sheath regions near the electrodes [3]. A smaller fraction of the applied voltage appears across the body of the plasma as a longitudinal electric field. The fraction of the applied voltage appearing across the sheaths depends upon many discharge parameters (e.g., pressure, RF frequency), and the fraction generally decreases with increasing ratio of negative ions to electrons. When the effective areas of the electrodes are not equal, one of the electrodes can also develop a large dc bias [4]. The division of the applied voltage between the sheath regions and the longitudinal electric field and the presence of the dc bias are important in describing the manner in which power is coupled into the discharge, and in describing the electron energy distribution function (EEDF). The EEDF in the RF discharges of interest have a large thermal group in which the bulk of the electrons reside, and a high-energy nonthermal tail which can extend for a few hundred electronvolts [5], [6]. The rates of electron collisions having high-energy thresholds (e.g., ionization) are sensitive to the details of the tail of the electron distribution function, and hence to the details of the sheath regions [7]. The large thermal group of electrons is excluded from the sheath regions and gains energy dominantly from the longitudinal electric field in the body of the plasma; that is, by joule heating.

The RF discharge simultaneously has characteristics of two very different types of discharges: the positive column and the hollow cathode [8]. In a positive column, power is coupled into the plasma by joule heating. By joule heating we mean the acceleration of electrons by the electric field in the plasma followed by an inelastic collision or velocity changing collision under conditions usually described as an electron swarm. The electron energy gained between collisions is usually a small fraction of the average electron energy. This process dominates in the body of our RF plasmas away from the electrodes. In the hollow cathode, power is coupled into the plasma by high-energy secondary electrodes (an e-beam component) emitted from the cathode [9]. This process is important in, and can dominate in, the sheath regions of our RF discharges. In this process, the emitted electron usually has its first collision after having been accelerated to an energy approximately equal to the sheath potential and successively slows down from this energy. A process intermediate to joule heating and the e-beam component, which we shall term electron "wave riding," is also in part responsible for the high-energy tail. Electron "wave

Manuscript received July 22, 1985; revised September 10, 1985. This work was supported by Spectra Technology, Inc.

The author is with Spectra Technology, Inc. (formerly Mathematical Sciences Northwest, Inc.), Bellevue, WA 98004.

IEEE Log Number 8406834.

0093-3813/86/0400-0188$01.00 © 1986 IEEE

riding,'' discussed in Section III, is the acceleration of low-energy thermal electrons during alternate half RF cycles by the oscillating sheaths [6], [10], [11]. The division of power deposition between the high-energy tail of the electron distribution and the large thermal group therefore dictates whether an RF discharge is best characterized as a positive column or a hollow cathode.

In Section II, the plasma simulation model will be briefly described, and in Section III, the EEDF in the RF discharges of interest will be discussed. Power deposition by electrons in these discharges will be examined in Section IV, and the spatial and time dependence of excitation rates will be studied in Section V. Concluding remarks are in Section VI.

II. Monte Carlo Simulation of Electron Properties in RF Discharges

A computer code has been developed [5], [12] which uses the Monte Carlo method to obtain the time- and spatially dependent EEDF in an RF capacitively coupled parallel-plate discharge. Results from this simulation will be used in this paper for our discussion of power deposition and excitation rates. Spatially dependent Monte Carlo techniques [13] are used in the parallel-plate geometry to compute electron trajectories and collision probabilities while oscillating the applied potential at RF frequencies. After oscillating the applied field for many RF cycles to reach steady-state conditions, the location, RF phase, and energy of the simulation particles are periodically recorded and summed to obtain the EEDF. By integrating over many RF cycles, the time-averaged spatially dependent EEDF is obtained. Typically, 1000 particles were used in the simulation, the energy and position of each particle were recorded 100 times per cycle, and the summation period was eight RF cycles after initially oscillating for five RF cycles to obtain the steady state. Details of the model are discussed in [5] and [12]. Pertinent aspects and revisions to the model will be discussed below.

In this study, we are interested in the parametric behavior of certain variables such as dc bias, longitudinal electric field in the plasma, and the rate of secondary emission. These variables are not independent, and in an experiment it is usually not possible to change only one parameter and be assured that the others remain fixed. It is this interdependence that makes the results of many experiments difficult to interpret. In order to isolate the effects of interest, in this paper we will vary only one parameter at a time. As a result, this treatment is not totally self-consistent with respect to the potential distribution between the electrodes. This approach has the advantage of isolating the changes in plasma properties wrought by the change in a given parameter; however, it lacks the self-consistency required for a true engineering design model.

The electron-impact rate constants discussed below were obtained by summing the electron collisions during the simulation. The time-averaged electron-impact rate constant is $k(x)$ ($\mathrm{cm}^3 \cdot \mathrm{s}^{-1}$) $= S_i(x)/(N_i \Delta t)$, where $S_i(x)$ is the sum of collisions of type i at location x, N_i is the density of the collision partner for process i, and Δt is the summation period (many RF cycles). Power deposition per average electron was obtained from

$$P_e = \sum_i \int_0^L \int_0^\infty f(\epsilon, x)\, \epsilon^{1/2} \left[\frac{2\epsilon}{m_e}\right]^{1/2} \sigma_i(\epsilon)\, \Delta\epsilon_i N_i \, d\epsilon\, dx \quad (1)$$

where ϵ is the electron energy, x is the position in the discharge, m_e is the electron mass, L is the electrode spacing, and $f(\epsilon, x)$ is the EEDF (units of $\mathrm{eV}^{-3/2} \cdot \mathrm{cm}^{-1}$). The sum is over electron collision processes having cross section $\sigma_i(\epsilon)$ and collision partner having density N_i. $\Delta\epsilon_i$ is the threshold energy for collision i for inelastic collisions, or $2m_e\epsilon/M_i$ for elastic collisions.

Secondary electron emission was included in the simulation by randomly choosing particles at the rate r_{SE} (see below) and placing the particles at a randomly chosen electrode with zero energy. These electrons are then accelerated into the plasma by the sheath potential. The sheath potential at an electrode is the maximum energy available to secondarily emitted electrons.

The voltage applied to the powered electrode is shared between the sheaths and the bulk plasma, where it appears as a longitudinal electric field. In the simulation

$$\begin{aligned} V_{\mathrm{RF}}(t) \sin [2\pi \upsilon_{\mathrm{RF}} t] &= [V_{s1}^{\mathrm{RF}} - V_{s2}^{\mathrm{RF}}] \sin [2\pi \upsilon_{\mathrm{RF}} t] + E_B(t) \\ &\quad \cdot [L - l_{s1}(t) - l_{s2}(t)] \end{aligned} \quad (2)$$

where the numeric subscripts identify an electrode, υ_{RF} is the RF frequency, and L is the electrode spacing. l_{si} is the sheath thickness and V_{si}^{RF} is the RF component of the sheath potential for electrode i (1 for powered electrode, 2 for grounded electrode). E_B is the magnitude of the longitudinal electric field in the bulk plasma

$$E_B(t) = E_0 \sin [2\pi \upsilon_{\mathrm{RF}} t]. \quad (3)$$

In our parametric model, l_s and E_0 are specified values. The thickness l_s was assumed to have both a dc and an RF component

$$l_{si}(t) = l_{si}^{\mathrm{dc}} + l_{si}^{\mathrm{RF}} \sin [2\pi \upsilon_{\mathrm{RF}} t]. \quad (4)$$

For the calculations discussed here, $l^{\mathrm{dc}} = 2.5$ mm and $l^{\mathrm{RF}} = 0.25$ mm for both electrodes. The dc value of the sheath thickness was estimated by solving for the electron and ion densities near a surface biased at the average sheath potential using the sheath model described in [14].

The sheath potential at an electrode is the difference between the potential of that electrode and the plasma potential. For capacitively coupled RF discharges, the sheath potential at the powered electrode is approximately

$$V_{s1}(t) = V_{\mathrm{dc}} + V_{\mathrm{RF}} \sin [2\pi \upsilon_{\mathrm{RF}} t] - V_p(t) - V_L(t) \quad (5)$$

where V_{dc} is the dc self- or applied bias, V_{RF} is the applied RF potential, V_p is the plasma potential adjacent to the grounded electrode, and V_L is the voltage drop asso-

ciated with the longitudinal electric field in the bulk plasma, equal to the last term in (2). For dominantly resistive or capacitive sheaths, the plasma potential can be written as [15]

$$\text{Resistive: } V_p(t) = \text{MAX}\,[V_{dc} + V^*_{RF} \sin [2\pi v_{RF} t], \Delta V]$$

$$\text{Capacitive: } V_p(t) = \text{MAX}\left[\frac{[V_{dc} + V^*_{RF}]}{2} \cdot [1 + \sin [2\pi v_{RF} t]], \Delta V\right] \quad (6)$$

where the function MAX (a, b) is the maximum of a and b, and ΔV is a small positive value approximately equal to the floating sheath potential. The asterisk for V^*_{RF} indicates a voltage amplitude less by an amount V_L than the applied voltage V_{RF}. For capacitively coupled discharges, $|V_{dc}| \leq V_{RF}$. The sheath potential at an electrode is generally negative unless the plasma has a high fraction of negative ions. The sheath potential at the grounded electrode is equal in magnitude, but opposite in sign, to the plasma potential. The sheath potential of the powered electrode V_{s2} is the difference between the plasma potential and the sum of the applied RF voltage and a dc self-bias. For the cases discussed in this paper, the resistive form for the plasma potential in (6) is used.

The electric field within the sheath was assumed to be linearly proportional to the distance from the edge of the plasma to the electrode. Recent spectroscopic measurements of the electric field within an RF sheath differ little from this form [3]. The electric field in the sheaths $E_s(t)$ in the simulation therefore had the form

$$E_{si}(x, t) = \frac{2V_{si}(t)\,[l_{si}(t) - x]}{l_{si}(t)^2} \quad (7)$$

where, again, the subscript i refers to electrode 1 or 2. The results from the simulation are not very sensitive to the shape of the electric field within the sheath.

For the discussion in this paper, we will examine gas mixtures of Ar and SiH_4, commonly used for the PECVD of amorphous silicon [2]. The cross sections used in the simulation for argon are from [16] (elastic scattering), [17] and [18] (electronic excitation), and [19] (ionization). For SiH_4, cross sections were obtained from [20] (dissociative ionization), [21] (total dissociation), [22] (momentum transfer, vibrational and electronic excitation), and [23] (attachment). The cross section for neutral dissociation of SiH_4 was assumed to be the difference between the total dissociation cross section and the dissociative ionization cross section. The effect of silane dissociation products on the electron distribution function has not been included in this analysis. The cross sections for the ionization of ground-state argon, the neutral dissociation of SiH_4, and the vibrational excitation of SiH_4 are plotted in Fig. 1. The rates for these three processes will be discussed below. These three processes were in particular chosen for detailed examination because they are processes representative of collisions having high-energy (argon ionization 16 eV), intermediate-energy (silane neutral dissociation 8 eV), and low-energy (silane vibrational excitation 0.1 eV) thresholds, and therefore have rates that respond to different portions of the EEDF.

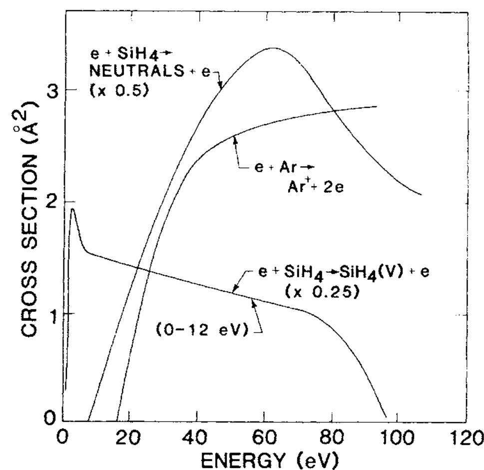

Fig. 1. Electron-impact cross sections used in the simulation for argon ionization, neutral dissociation of SiH_4, and vibrational excitation of SiH_4. The energy scale for vibrational excitation has been expanded by a factor of 10 and spans 0–12 eV.

III. EEDF's in Ar/SiH_4 Plasmas

Typical time-averaged electron energy distributions obtained with the simulation as a function of position between the electrodes in an RF parallel-plate discharge operating at 12 MHz are plotted in Fig. 2. The gas mix is SiH_4/Ar:0.1/0.9, the gas pressure is 70 mtorr, and the electrode separation is 2.4 cm. The powered electrode is at $x = 0$ cm, and the grounded electrode is at $x = 2.4$ cm. The RF amplitude is 75 V and the dc biases at the powered electrode for the two cases plotted in Fig. 2(a) and (b) are -45 V and 0 V, respectively. The amplitude of the electric field in the bulk plasma is $E_0 = 10$ V/cm (electric field/number density $(E/N) = 440$ Td, 1 Td $= 1 \times 10^{-17}$ V $\cdot$ cm^2). The quantity plotted is $\log_{10}(f(\epsilon, x)\,\text{eV}^{-3/2} \cdot \text{cm}^{-1})$. Note that the majority of the electrons reside at energies less than about 10 eV in a largely thermal group. The spatially averaged electron temperature for both cases is 2.0 eV. Near the electrodes are long high-energy tails to the EEDF. The high-energy tail is most prominent near the powered electrode in the presence of the dc bias. Although the majority of the electrons in the tail of the distribution slow down close to the powered electrode, a fraction survive to traverse the plasma and are collected by the opposite electrode. The high-energy limit to the tail of the distribution is a value approximately equal to the maximum sheath potential. This value is lower in absence of the dc bias at the powered electrode. The EEDF is symmetric about the centerline of the discharge in the absence of the dc bias, a reflection of the symmetric potential distribution. Note that at the grounded electrode, the tail to the distribution extends to a higher energy in the absence of the dc bias than with the dc bias. This results from a lowering of the average sheath poten-

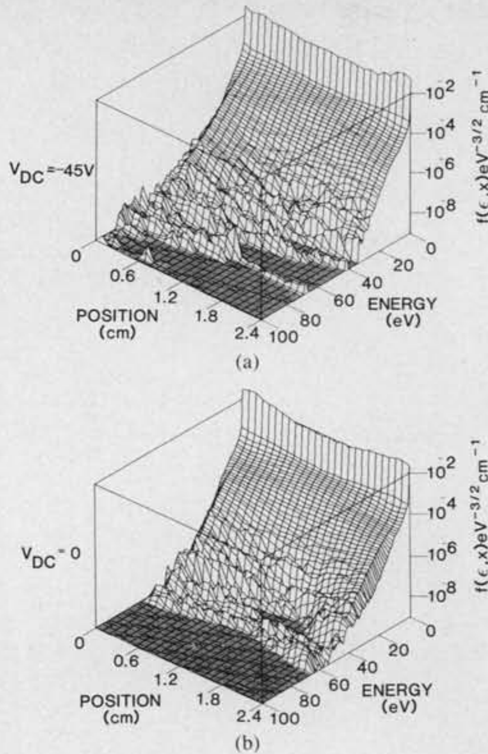

Fig. 2. Typical electron distribution functions for an RF discharge (12 MHz) in a 70-mtorr mixture of Ar/SiH$_4$: 0.9/0.1. The quantity plotted is $\log_{10}(f(\epsilon, x)\ \mathrm{eV}^{-3/2} \cdot \mathrm{cm}^{-1})$. The applied RF voltage amplitude is 75 V: (a) dc bias on the powered electrode ($x = 0$) of -45 V; (b) $V_{dc} = 0$.

tial at the grounded electrode with a negative dc bias on the powered electrode.

The thermal group of electrons which dominates the bulk plasma is characterized by a temperature which is in large part a function of the electric field in the bulk of the plasma, as will be discussed in Section IV. The high-energy tail of the EEDF near the electrodes, though, results from at least two processes: secondary electrons and "wave riding" electrons. We will first discuss the source of secondary electrons.

Ions which diffuse out of the plasma and into the sheaths are accelerated into the electrodes and cause secondary emission of electrons. The secondarily emitted electrons are in turn accelerated back into the plasma, and carry with them an energy nearly equal to the sheath potential. The rate at which secondary emission occurs R_{SE} ($\mathrm{cm}^{-2} \cdot \mathrm{s}^{-1}$) is approximately

$$R_{SE} = \left[\frac{\gamma D^* N_I}{\Lambda^2}\right]\left[\frac{V}{A}\right] \tag{8}$$

where γ is the secondary emission coefficient, Λ is the diffusion length of the reactor, D^* is the positive ion diffusion coefficient, and N_I is the density of positive ions. The volume of the plasma is V, and the total area of the electrodes is A. The superscript * denotes that the value of the diffusion coefficient is between the free diffusion coefficient and the ambipolar diffusion coefficient as given by the Bohm limit [24]. An accurate self-consistent accounting of secondary electron emission requires a more

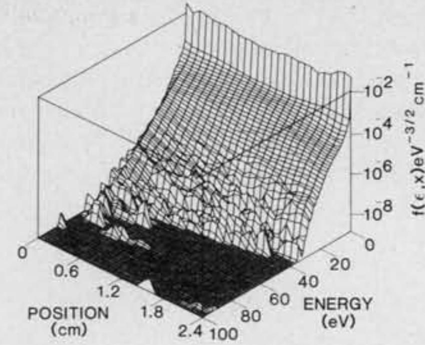

Fig. 3. Electron distribution function for the conditions of Fig. 2(a) where secondary electron emission is excluded. The highest energy electrons in the tail of Fig. 2(a) are seen to be due to secondary emission; the majority of the high-energy electrons are due to wave riding.

detailed kinetic analysis of the transport of ions than was performed for this study. Therefore, in our analysis, the rate of secondary electron emission *per electron* in the discharge r_{SE} was treated as a parametric variable. (r_{SE} is related to R_{SE} by $r_{SE} = R_{SE}/LN_I$.) The value of r_{SE} also depends upon the fractional density of negative ions. For electronegative plasmas, $N_I^+ \approx N_I^- >> n_e$ so that r_{SE} can be large. For the electron distributions plotted in Fig. 2, $r_{SE} = 10^5\ \mathrm{s}^{-1}$, appropriate for Bohm diffusion with $\gamma = 0.15$.

Secondary emission is not the only source of electrons in the high-energy tail of the distribution; another source is "wave riding" electrons. The sheath at the electrodes in an RF discharge can oscillate in either space, energy, or both [10], [25]. Spatial oscillation occurs when the boundary between the sheath and the plasma physically changes its location with respect to the electrode during an RF cycle. Energetic oscillation occurs when the sheath potential changes during an RF cycle. In either case, the local plasma potential oscillates. During that portion of the RF cycle when the sheath is in retreat, either spatially or energetically, the plasma potential near and in the sheath increases. During this portion of the RF cycle, thermal electrons from the plasma diffuse or drift toward the electrodes. During the second half of the RF cycle, the sheath spatially or energetically extends back into the plasma. The electrons that followed the sheath in its retreat towards the electrode suddenly find themselves in a region with a lower plasma potential. These largely thermal electrons are then accelerated into the plasma, riding the wave of the lower plasma potential. The energy gained by an electron which is in the path of the extending sheath is approximately equal to the difference between the minimum potential and plasma potential at the location of the electron's closest approach. The result is a broad high-energy tail to the EEDF located at the boundary of the sheath and the plasma. This mechanism, different from joule heating or secondary electron emission, may be identified with that discussed by Godyak, who describes a collisionless absorption of power by electrons that is associated with the oscillation of the sheaths [6], [10], [11].

In Fig. 3 is the EEDF for identical conditions to the

case of $V_{dc} = -45$ V in Fig. 2, except that $\gamma = 0$. A broad high-energy tail is present even in the absence of secondary emission, due to electron wave riding. Note that the highest energy electrons, with energies equal to the maximum amplitude of the sheath potential, result from secondary emission. A larger fraction of electrons in the tail, though, are "wave riders."

IV. Power Deposition

Power is coupled into the RF discharge by electrons in at least two ways: secondary electrons emitted at the surface of the electrodes (or wave riding electrons) are accelerated into the plasma, carrying with them an energy at most equal to the sheath potential; and electrons in the body of the plasma are heated by the bulk longitudinal electric field. To the extent that the former process is dominant, the RF discharge resembles a hollow cathode. To the extent that the latter process is dominant, the RF discharge mimics a positive column. To examine the method of power deposition, we will separately vary the dc sheath potential, RF voltage, and bulk longitudinal electric field in the simulation and examine the change in power deposition and excitation rates that results.

While keeping other quantities fixed, we varied the amplitude of the longitudinal electric field in the bulk plasma (E_0). The results are plotted in Fig. 4 for RF amplitudes of 75 and 125 V for cases with and without a dc bias ($V_{dc} = -0.6 \cdot V_{RF}$). The discharge conditions are similar to those for Fig. 2 except that P = 135 mtorr. In Fig. 4(a), power deposition P_e and the enhancement to P_e with a dc bias are plotted. For an electron density of 10^9 cm^{-3}, power deposition is approximately 2.5 mW $\cdot$ cm^{-3} with E_0 = 5 V/cm (100 Td), increasing to approximately 22 mW $\cdot$ cm^{-3} with E_0 = 22.5 V/cm^{-3} (520 Td) [26],[1] [27].[2] The incremental increase in P_e when changing V_{RF} is relatively constant regardless of E_0, as is the enhancement due to the dc bias. This is a result of the constant value of secondary electron emission and constant fraction of electrons subject to wave riding. The fraction of P_e due to sheath processes is therefore larger at the smaller values of E_0. The enhancement in P_e with a dc bias, resulting from sheath-associated power deposition processes, is as large as 200 percent at low E_0, decreasing to 10 percent with high E_0. The volume-averaged electron temperature and excitation rates for argon ionization and silane neutral dissociation are plotted in Fig. 4(b). For a given value of E_0, the electron temperature is nearly independent of V_{RF}

[1]An electron density of a few times 10^9 cm^{-3} is typical for RF plasmas having power densities of a few to tens of mW $\cdot$ cm^{-3}. Recent measurements using microwave transmission spectroscopy of the electron density of 13.56-MHz plasmas sustained in CHF_3, Ar, and O_2 yielded values in the range of 2-7 $\times$ 10^9 cm^{-3} for power densities of 10-90 mW $\cdot$ cm^{-3}.

[2]Measurements of the electron density of dc and pulsed hollow cathode discharges sustained in He/SiH_4 mixtures have recently been made using microwave interferometry. The range of power deposition was P = 8-80 mW $\cdot$ cm^{-3} and the silane mole fraction was M = 0.01-0.04. The average electron density was found to be linearly proportional to the discharge current and inversely proportional to the silane mole fraction. The measured electron density is in the range of 2-12 $\times$ 10^9 cm^{-3} for 0.01 < M < 0.04 and $P \approx$ 15 mW $\cdot$ cm^{-3}.

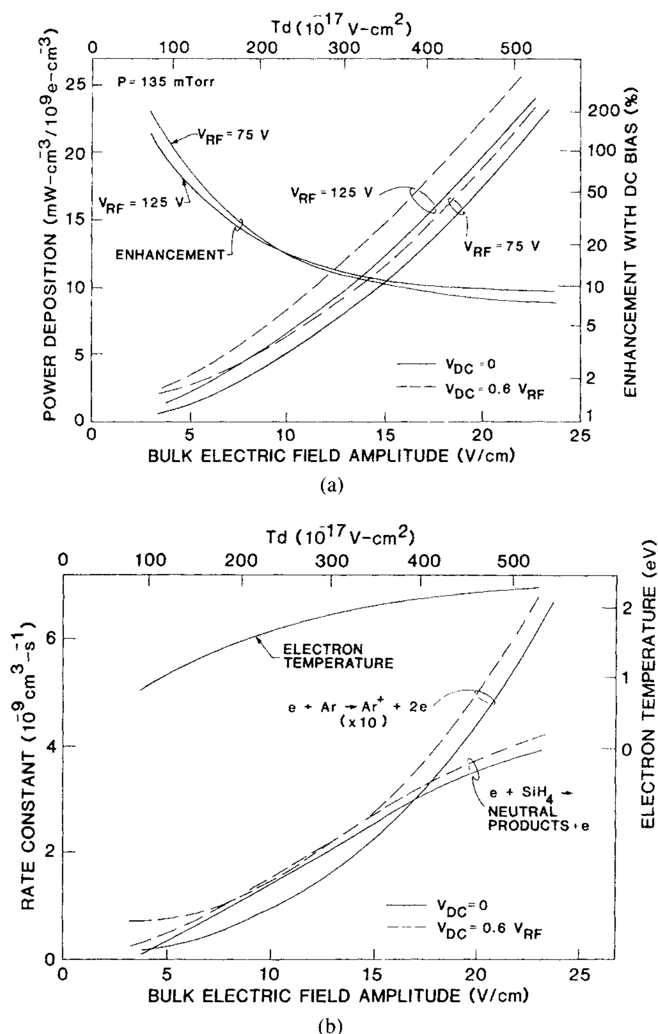

Fig. 4. Discharge properties as a function of bulk electric-field amplitude E_0 for P = 135 mtorr. Cases with V_{RF} = 75 and 125 V are shown, with and without a dc bias: (a) electron power deposition ($n_e = 10^9$ cm^{-3}) and enhancement in power deposition with a dc bias; (b) electron temperature and excitation rates for V_{RF} = 75 V.

(with or without a dc bias); that is, the temperature of the bulk electrons depends only on the value of E_0. Power deposition by sheath processes appears to dominate for E_0 < 5-10 V/cm (E_0 < 100-200 Td). For these smaller values of E_0, power deposition is dominated by the less numerous high-energy electrons in the tail of the distribution rather than by the more numerous bulk electrons which determine the average electron temperature. As E_0 increases, high-energy (Ar ionization) and intermediate-energy (SiH_4 neutral dissociation) threshold events have volume-averaged excitation rates that are generally functions of only E_0 unless r_{SE} is also large (>10^6 s^{-1}) (see discussion below). The spatial dependence of these rates, though, depends on properties other than E_0, as will be discussed in Section V.

The degree to which V_{RF} and V_{dc} influence power deposition *when E_0 remains constant* is shown in Fig. 5 where power deposition P_e and its enhancement with a dc bias ($V_{dc} = -0.6 \cdot V_{RF}$) are plotted. Only small changes in P_e occur when changing the applied potential with constant E_0. This result implies that changes in power depo-

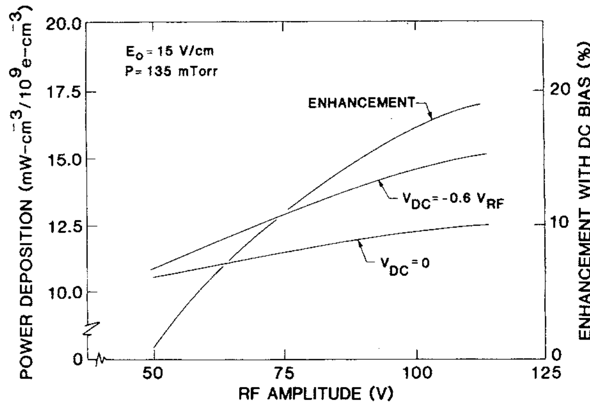

Fig. 5. Electron power deposition (n_e = 10^9 cm^{-3}) and enhancement in power deposition as a function of V_{RF}. The bulk electric-field amplitude is E_0 = 15 V/cm (350 Td).

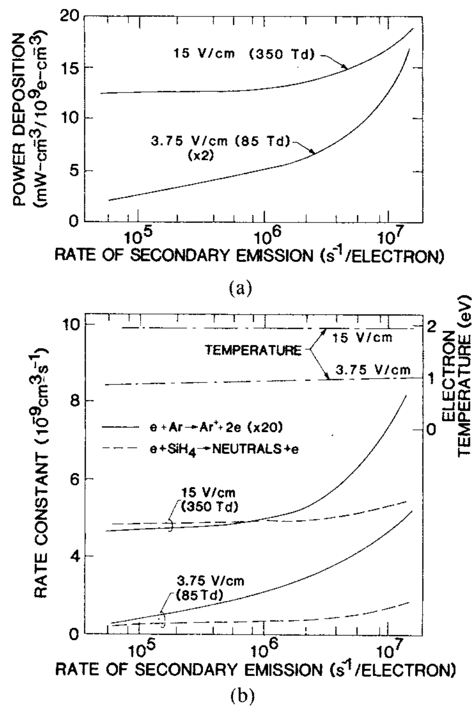

Fig. 6. Discharge properties as a function of the rate of secondary electron emission r_{SE} (emission/electron-s) for P = 135 mtorr. Cases for E_0 = 15 and 3.75 V/cm (350 and 85 Td) are plotted: (a) electron power deposition (n_e = 10^9 cm^{-3}); (b) electron temperature and excitation rates.

sition when increasing V_{RF} result dominantly from an increase in E_0 once $E_0 > 150$ Td. Fractional increases in P_e resulting from increasing V_{RF} alone are larger with smaller E_0 (< 150 Td). These results, though, depend on the rate of secondary electron emission. The effect of secondary electron emission on P_e is plotted in Fig. 6(a) for two values of E_0; 3.75 V/cm (75 Td) and 15 V/cm (300 Td). The independent parameter is the rate secondary emission per average electron r_{SE}. The results discussed above were obtained with $r_{SE} = 10^5$ s^{-1}. For $r_{SE} < 10^6$ s^{-1}, only a small increase in P_e occurs with increasing r_{SE}. The fractional increase in P_e is larger at low E_0. Only for values of $r_{SE} > 10^6$ s^{-1} does P_e begin to significantly change. As r_{SE} increases, the increase in P_e results dominantly from increases in the rate of high-energy deposition processes, as shown by the plot of excitation rates for argon ionization and silane neutral dissociation in Fig. 6(b). The implication of this exercise is that for these conditions, the majority of power deposition resulting from processes associated with the sheaths is due to the wave riding effect, and not necessarily secondary electron emission. This is due to the fact that the fraction of bulk electrons that can be wave riders is approximately $2l_s/L$, which is a much larger fraction than that which is secondarily emitted. Over the range of secondary electron emission coefficients plotted in Fig. 6(b), the electron temperature is nearly constant even though power deposition increases with increasing secondary emission. This is again an indication that, for increasing secondary emission, power deposition is dominated by less numerous high-energy electrons, whereas the average electron energy is determined by the more numerous low-energy bulk electrons.

In summary, for the examples studied here, power is dominantly coupled into the discharge by electrons as a result of joule heating in the bulk plasma when $E_0 > 150$ Td. When $E_0 > 150$ Td, the power per electron deposited within the bulk is still small ($\approx$ 4 eV/RF cycle) as compared to secondary or wave riding electrons (10–100 eV per event). The larger density of thermal electrons and the low rate of secondary emission, though, results in the majority of power being deposited, analogous to a positive column, as joule heating. Only for $E_0 < 150$ Td is power dominantly deposited as a result of sheath processes. Wave riding electrons appear to be the dominant form of power deposition by electrons for the sheath.

The value of the expected electric field in the bulk plasma ($E_0 \leq 20$ V/cm) is presently below the detection limit using spectroscopic techniques [3]. An estimate, though, can be made for the value of the self-consistent electric field by equating the time-averaged rates of generation and loss of positive and negative ions [8]. The importance, in this context, of negative ions in silane discharges has only recently been emphasized by DeJoseph *et al.* [28]. As shown below, the self-consistent bulk electric field E_0 is in large part determined by the fraction of negative ions.

To obtain an estimate of the self-consistent value of E_0, we assume that the negative and positive ion densities are given by their quasi-steady-state values. Using volume average rate constants, we approximate the rates for the negative ion density N^- and positive ion density N^+ as

$$\frac{dN^+}{dt} = 0 = n_e r_I N - N^- N^+ r_N - N^+ R_D \quad (9)$$

$$\frac{dN^-}{dt} = 0 = n_e r_A N - N^- N^+ r_N \quad (10)$$

where the electron density is n_e, and the appropriate neutral density is N. The rate constants for ionization, ion–ion neutralization, and attachment are r_I, r_N, and r_A, respectively. The rate of diffusion of positive ions is R_D. Negative ions cannot traverse the sheath ($T_{ion} << T_e$) and are lost only by ion–ion neutralization. Introducing the parameter $\alpha = N^-/n_e$, (9) and (10) yield

$$[r_I - r_A] N = (1 + \alpha) R_D \tag{11}$$

$$\alpha = \frac{1}{2}\left[\left[1 + \frac{4 r_A N}{r_N n_e}\right]^{1/2} - 1\right]. \tag{12}$$

The rate of diffusion is assumed to be given by the Bohm value. For a mixture of negative and positive ions, R_D is approximated by

$$R_D \approx \frac{3 \times 10^5}{L} \cdot \left[\frac{T_e + \alpha T_I}{1 + \alpha}\right]^{1/2} \text{s}^{-1} \tag{13}$$

where the electrode separation is L (cm), and the electron and ion temperatures are T_e and T_I (eV), respectively. The time- and volume-averaged rate constants r_I and r_a and the electron temperature T_e were obtained directly from the plasma simulation and are largelyfunctions of E_0. The rate constant for ionization is the mole fraction weighted sum of the rate constants for ionization of Ar and SiH_4. For $V_{dc} = 0$, this value ranges from 2.7×10^{-11} $cm^3 \cdot s^{-1}$ at $E_0 = 3.75$ V/cm (85 Td) to 1.0×10^{-9} $cm^3 \cdot s^{-1}$ at $E_0 = 22.5$ V/cm (520 Td). The attachment rate constant ranged from 1.0×10^{-11} $cm^3 \cdot s^{-1}$ at $E_0 =$ 3.75 V/cm to 5.0×10^{-11} $cm^3 \cdot s^{-1}$ at $E_0 = 22.5$ V/cm. The rate constant for attachment inferred from recent measurements of the electron density in the afterglow of a pulsed hollow cathode discharge in an He/SiH_4 mixture is significantly larger; however, the attachment is attributed to a dissociation product of SiH_4.[3] The mole fraction weighted rate constant for attachment (SiH_4 mole fraction 0.1) is 1.0-5.0 $\times 10^{-12}$ $cm^3 \cdot s^{-1}$. The value of r_N was approximated as 10^{-7} $cm^3 \cdot s^{-1}$ [29].

For a specified value of electronegativity α a self-consistent value for E_0 is obtained by satisfying (11). A self-consistent value of α is obtained from (12) by specifying an electron density. The values for E_0 and α obtained in this fashion are plotted in Fig. 7. The conditions are the same as those for Fig. 4. For $V_{dc} = 0$ and $\alpha = 0$, the self-consistent bulk electric field is $E_0 = 3.5$ V/cm (80 Td), a value corresponding to electron power deposition being dominated by sheath processes. The values of α for which power deposition by electrons is dominated by sheath processes (low E_0) and power deposition is dominated by bulk processes (high E_0) are $\alpha < 10$ and $\alpha > 10$, respectively. Estimating that the electron density [26],[1] [27][2] lies in the range 10^9 $cm^{-3} \le n_e \le 10^{10}$ cm^{-3}, the self-consistent values of E_0 lie predominantly at values of $\alpha < 10$; that is, in a region where power deposition by electrons is dominated by sheath processes. Since high-energy threshold processes such as ionization are enhanced in the presence of a dc bias, the self-consistent electric field amplitude is lower for a given α with a dc bias compared to the

[3]The attachment rate in the afterglow of a pulsed hollow cathode discharge in an He/SiH_4 gas mixture has been inferred from measurements of the decay in electron density (see [27]). A lower bound on the rate coefficient of 2.65×10^{-10} $cm^3 \cdot s^{-1}$ was determined; however, the attaching species was theorized as being a dissociation product of SiH_4. This value for the attachment coefficient is an order of magnitude larger than one obtains using the dissociative attachment cross section for SiH_4 of [23], which has peak value of only 3×10^{-18} cm^2.

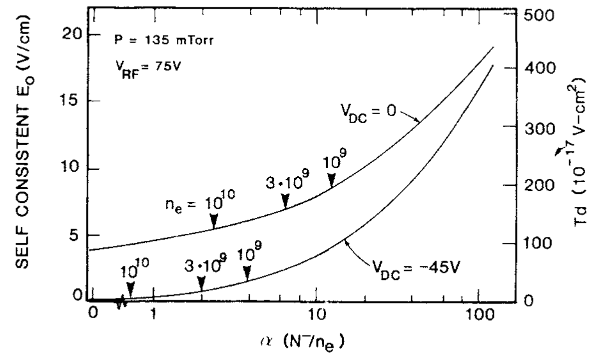

Fig. 7. Self-consistent values of the bulk electric-field amplitude E_0 obtained by balancing the rate of generation and loss of ions. The parameter α is the ratio N^-/n_e (negative ion density/electron density). Values of α < 10 yield values of E_0 that suggest power deposition is dominated by sheath processes. By specifying the electron density, a unique relationship between α and E_0 can be obtained.

same conditions without a dc bias. Electron power deposition with a dc bias ($V_{dc} = -45$ V) is dominated by sheath processes for $\alpha < 30$. For 10^9 $cm^{-3} \le n_e \le$ 10^{10} cm^{-3}, the self-consistent values of E_0 lie entirely at values of $\alpha < 10$ where power deposition by electrons is dominated by sheath processes.

V. Spatial Dependence of Excitation Rates

The spatial- and time-dependent density of excited species within RF discharges have been studied experimentally [25], [30]-[32] and have been shown to have complex behavior. In Section IV, we found that for sufficiently large values of the bulk electric field, power deposition by electrons results primarily from joule heating in the bulk of the plasma and is spatially fairly uniform. The spatial distributions of excitation rates for processes with high-energy thresholds, though, are not uniform. This spatial nonuniformity is sensitive to changes in the sheath characteristics.

The degree to which the presence or absence of a dc bias on the powered electrode effects the spatial distributions of excitation rates is illustrated in Fig. 8, where the excitation rates for the ionization of argon, neutral dissociation of SiH_4, and vibrational excitation of SiH_4 are plotted. The two figures are for cases with and without a dc bias ($V_{RF} = 75$ V, $V_{dc} = -45$ V, $E_0 = 15$ V/cm (350 Td), $P = 135$ mtorr). The excitation rate for vibrational excitation is approximately constant as a function of position and is relatively insensitive to the value of V_{dc}, a consequence of the fact that vibrational excitation results from collisions with the low-energy electrons in the bulk of the plasma. The higher energy threshold processes for SiH_4 dissociation and argon ionization (threshold energies 8 and 16 eV, respectively), though, have excitation rates whose spatial distributions are sensitive to the dc bias. For the case where $V_{dc} = 0$, these excitation rates are fairly symmetric about the midplane with local maxima near the electrodes. With $V_{dc} = -45$ V, a sharp peak in the high threshold rates occurs near the powered electrode, a consequence of the enhanced high-energy tail to the EEDF. The fractional increase in the Ar^+ rate exceeds

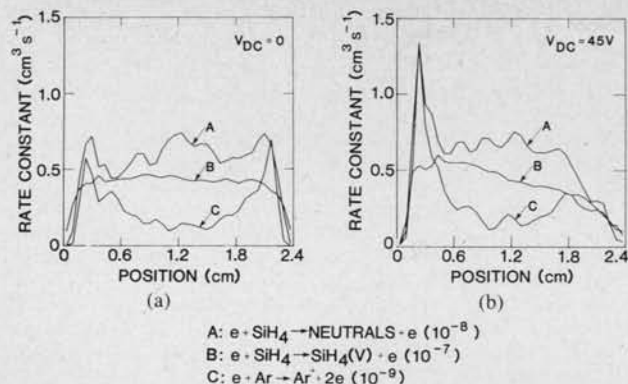

Fig. 8. Electron-impact excitation rate constants for argon ionization (A), vibrational excitation of SiH_4 (B), and neutral dissociation of SiH_4 (C) as a function of position between the electrodes for conditions similar to those in Fig. 4 with E_0 = 15 V/cm (350 Td): (a) V_{dc} = 0; (b) V_{dc} = −45 V.

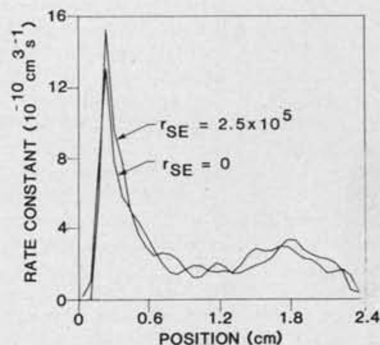

Fig. 9. Electron-impact excitation rate constant for argon ionization as a function of position between the electrodes with and without secondary electron emission.

that of the SiH_4 dissociation rate due to the higher threshold energy for ionization. The local enhancement in high threshold excitation is due in large part to the wave riding effect. The rate of argon ionization is plotted in Fig. 9 for cases with and without secondary emission. For these conditions, only a nominal increase in the rate occurs when secondary emission is included. Only when r_{SE} is large ($>10^6\ s^{-1}$) can the enhancement in the local rate constant be attributed primarily to secondary emission.

For electron collisions that have an intermediate energy threshold, such as neutral dissociation of SiH_4 (ϵ = 8 eV), local extrema in the rate constants are a consequence of sheath processes. The majority of the excitation collisions, though, result from collisions with the bulk low-temperature electrons. The rate constants for neutral dissociation and vibrational excitation of SiH_4 are plotted in Fig. 10 for different values of E_0 (V_{RF} = 75 V, V_{dc} = 0, P = 135 mtorr). The rate of vibrational excitation is relatively constant for this range of E_0. The rate of dissociation, initially largest near the sheaths at low E_0, increases throughout the discharge because of the increase in the average energy of the bulk electrons (1.4 eV $\le kT_e \le$ 2.4 eV).

The spatially dependent excitation rates discussed thus far are time averaged over many RF cycles. The nonuni-

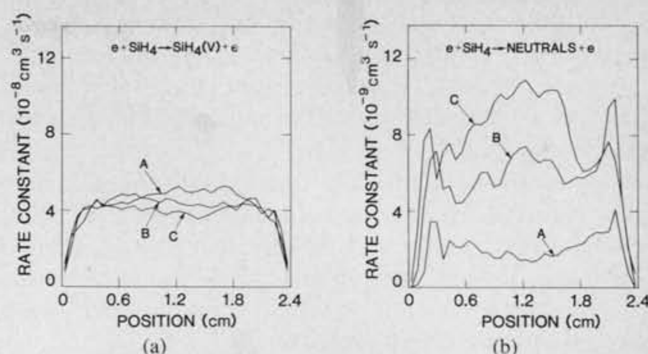

Fig. 10. Electron-impact excitation rate constants for (a) vibrational excitation of SiH_4, and (b) neutral dissociation of SiH_4 as a function of position between the electrodes (V_{dc} = 0) for different values of the bulk electric-field amplitude: $A \equiv$ 7.5 V/cm (175 Td); $B \equiv$ 15 V/cm (350 Td); $C \equiv$ 22.5 V/cm (525 Td).

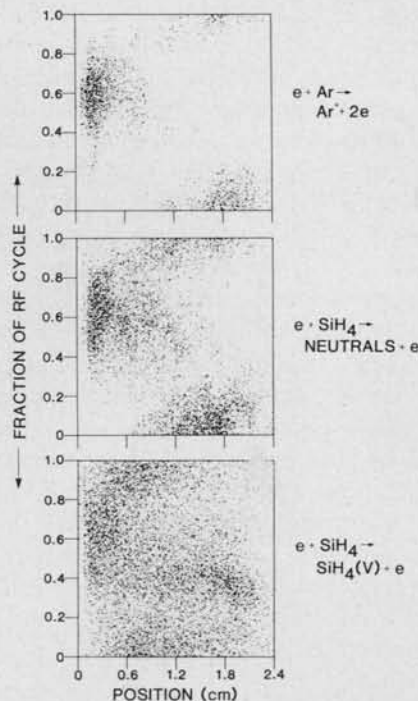

Fig. 11. Excitation rates as a function of position between the electrodes (V_{dc} = −45 V) and phase in the RF cycle for argon ionization (top), neutral dissociation of SiH_4 (middle), and vibrational excitation of SiH_4 (bottom). The density of dots is proportional to the rate of excitation. Each plot has been separately normalized.

formity of excitation rates is also a function of phase in the RF cycle. Examples of temporal nonuniformity appear in Fig. 11 where the relative occurrence of collisions as computed with the simulation is plotted as a function of space and time. The conditions are the same as in Fig. 8(b). The density of dots in Fig. 11 is proportional to the rate of collisions at a particular location and time. The applied RF voltage is at its minimum value (voltage = $-V_{RF}$) at 0.5 in the RF cycle as indicated in Fig. 11. Each collision process is separately normalized. The nonuniformity of excitation is greatest for high threshold energy processes, and least for low threshold energy processes. This pattern is a result of the tail of the EEDF being mod-

ulated during the RF cycle while the bulk electron temperature remains relatively constant during the RF cycle. A similar conclusion on the disparity in the modulation of the tail of the distribution, as compared to the bulk, was discussed by Vagner *et al.* [7].

When power is dominantly coupled into the discharge via the bulk electric field as joule heating, the deposition is fairly spatially uniform. Spatially dependent excitation phenomena, though, can simultaneously occur when the characteristics of the tail of the distribution function are dominated by the sheath processes.

VI. Conclusion

For the conditions examined in this paper (70–150 mtorr Ar/SiH_4: 0.9/0.1, $V_{RF} < 150$ V) power deposition is dominated by sheath processes when the amplitude of the oscillating electric field in the bulk plasma E_0 is less than 150 Td. For $E_0 > 150$ Td, power deposition by electrons increases significantly only when the longitudinal electric field in the plasma increases. By equating the rates for generation and loss of ions, one can estimate a self-consistent value of E_0. When $V_{dc} = 0$, the self-consistent value of $E_0 < 150$ Td when $\alpha = N^-/n_e < 10$, and $E_0 > 150$ Td when $\alpha > 10$. The corresponding breakpoint for $V_{dc} = -45$ V is $\alpha = 30$. When stipulating that the electron density is in the range 10^9 cm$^{-3} \leq n_e \leq 10^{10}$ cm^{-3}, the self-consistent value of E_0 implies that power deposition by electrons is dominated by sheath processes. For our conditions, the majority of power deposited by electrons from sheath processes results from "wave riding" electrons rather than from secondary emission. Although for some conditions a large fraction of power deposition may occur uniformly from joule heating in the bulk plasma, spatially and temporally nonuniform excitation rates can simultaneously occur for high threshold energy collisions as a result of sheath-associated modulation of the tail of the distribution function.

References

[1] J. W. Coburn and H. F. Winters, "Plasma-assisted etching in microfabrication," *Ann. Rev. Mater. Sci.*, vol. 13, pp. 91-116, 1983.

[2] F. J. Kampas, "Chemical reactions in plasma deposition," *Semicond. and Semimetals*, vol. 21A, pp. 153-177, 1984.

[3] C. A. Moore, G. P. Davis, and R. A. Gottscho, "Sensitive nonintrusive, in-situ measurement of temporally- and spatially-resolved plasma electric fields," *Phys. Rev. Lett.*, vol. 52, pp. 538-541, 1984.

[4] H. R. Koenig and L. I. Maissel, "Applications of RF discharges to sputtering," *IBM J. Res. Develop.*, vol. 14, pp. 168-171, 1970.

[5] M. J. Kushner, "Monte-Carlo simulation of electron properties in RF parallel plate capacitively coupled discharges," *J. Appl. Phys.*, vol. 54, pp. 4958-4965, 1983.

[6] V. A. Godyak and S. N. Oks, "Electron distribution in a low-pressure RF discharge," *Sov. Phy.—Tech. Phys.*, vol. 24, pp. 1255-1256, 1979.

[7] S. D. Vagner, B. K. Ignat'ev, and L. D. Tsendin, "Modulation of the emission of a neon RF discharge due to time variation of the fast-electron distribution," *Sov. Phys.—Tech. Phys.*, vol. 23, pp. 665-666, 1978.

[8] J. H. Keller and W. B. Pennebaker, "Electrical properties of RF sputtering systems," *IBM J. Res. Develop.*, vol. 23, pp. 3-15, 1979.

[9] B. E. Warner, K. B. Persson, and G. J. Collins, "Metal-vapor production by sputtering in a hollow-cathode discharge: Theory and experiment," *J. Appl. Phys.*, vol. 50, pp. 5694-5703, 1979.

[10] O. A. Popov and V. A. Godyak, "Power dissipated in low-pressure radio-frequency discharge plasmas," *J. Appl. Phys.*, vol. 57, p. 53-58, 1985.

[11] V. A. Godyak, "Steady-state low-pressure RF discharge," *Sov. J. Plasma Phys.*, vol. 2, pp. 78-84, 1976.

[12] M. J. Kushner, H. Anderson, and P. J. Hargis, Jr., "Simulation of time and spatially dependent excitation processes in RF discharges for plasma processing," in *Plasma Synthesis and Etching of Electronic Materials*, vol. 38, *Mater. Res. Soc. Symp. Proc.* Pittsburgh, PA: Mater. Res. Soc., 1985, pp. 201-214.

[13] Examples of early and recent applications of the Monte Carlo method to electron swarms can be found in: J. Lucas, "A theoretical calculation of electron swarm properties in helium," *Int. J. Electron.*, vol. 32, pp. 393-410, 1972; and
J. P. Boeuf and E. Marode, "Monte Carlo simulation of electron swarm motion in SF_6," *J. Phys. D*, vol. 17, 1133-1148, 1984.

[14] M. J. Kushner, "Floating sheath potentials in non-Maxwellian plasmas," *IEEE Trans. Plasma Sci.*, vol. PS-13, pp. 6-9, 1985.

[15] K. Kohler, J. W. Coburn, D. E. Horne, and E. Kay, "Plasma potentials of 13.56-MHz argon glow discharges in a planar system," *J. Appl. Phys.*, vol. 57, pp. 59-66, 1985.

[16] M. Hayashi, "Recommended values of transport cross sections for elastic collision and total collision cross section for electrons in atomic and molecular gases," Nagoya Inst. of Tech., Nagoya, Japan, Rep. IPPJ-AM-19, 1981.

[17] F. J. de Heer, R. H. J. Jansen, and W. van der Kaay, "Total cross sections for electron scattering by Ne, Ar, Kr and Xe," *J. Phys. B.*, vol. 12, pp. 979-1002, 1979.

[18] H. N. Kucukarpaci and J. Lucas, "Electron swarm parameters in argon and krypton," *J. Phys. D*, vol. 14, pp. 2001-2014, 1981.

[19] D. Rapp and P. Englander-Golden, "Total cross sections for ionization and attachment in gases by electron impact," *J. Chem. Phys.*, vol. 43, pp. 1464-1479, 1965.

[20] H. Chatham, D. Hils, R. Robertson, and A. Gallagher, "Total and partial electron collision ionization cross sections for CH_4, C_2H_6, SiH_4, and Si_2H_6," *J. Chem. Phys.*, vol. 81, p. 1770, 1984.

[21] J. Perrin, J. P. M. Schmitt, G. De Rosny, B. Drevillon, J. Huc, and A. LLoret, "Dissociation cross sections for silane and disilane by electron impact," *Chem. Phys.*, vol. 73, pp. 383-394, 1982.

[22] A. Garscadden, G. L. Duke, and W. F. Bailey, "Electron kinetics of silane discharges," *Appl. Phys. Lett.*, vol. 43, p. 1012, 1983.

[23] V. H. Ebinghaus, K. Kraus, W. Muller-Duysing, and H. Neuert, "Negative ionen durch elektronenresonanzeinfang in PH_3, AsH_3 and SiH_4," *Z. Naturforsch.*, vol. 19a, pp. 732-736, 1964.

[24] B. Chapmann, *Glow Discharge Processing*. New York: Wiley, 1980.

[25] R. A. Gottscho, R. H. Burton, D. L. Flamm, V. M. Donnelly, and G. P. Davis, "Ion dynamics of RF plasmas and plasma sheaths: A time-resolved spectroscopic study," *J. Appl. Phys.*, vol. 55, p. 2707, 1984.

[26] C. A. M. de Vries, A. J. Roosmalen, and G. C. C. Puylaert, "Microwave spectroscopic measurements of the electron density in a planar discharge: Relation to reactive-ion etching of silicon dioxide," *J. Appl. Phys.*, vol. 57, pp. 4386-4390, 1985.

[27] C. B. Fleddermann, J. H. Beberman, and J. T. Verdeyen, "Measurement of the electron density and attachment rate coefficient in silane/helium discharges," *J. Appl. Phys.*, vol. 58, pp. 1344-1348, 1985.

[28] C. A. DeJoseph, Jr., P. D. Haaland, and A. Garscadden "Basic processes in silane discharges," in *Proc. 1985 IEEE Int. Conf. Plasma Sci.* (New York, NY), 1985, p. 13.

[29] A. P. Hickman, "Approximate scaling formula for ion–ion mutual neutralization rates," *J. Chem. Phys.*, vol. 70, pp. 4872-4878, 1979.

[30] G. De Rosny, E. R. Mosburg, Jr., J. R. Abelson, G. Devaud, and R. C. Kerns, "Evidence for a time dependent excitation process in silane radio frequency glow discharges," *J. Appl. Phys.*, vol. 54, p. 2272, 1983.

[31] R. M. Roth, K. G. Spears, and G. Wong, "Spatial concentrations of silicon atoms by laser-induced fluorescence in a silane glow discharge," *Appl. Phy. Lett.*, vol. 45, pp. 28-30, 1984.

[32] R. A. Gottscho, G. P. Davis, and R. H. Burton, "Spatially resolved laser-induced fluorescence and optical emission spectroscopy of carbon tetrachloride glow discharges," *Plasma Chem. Plasma Proc.*, vol. 3, pp. 193-217, 1983.